

***Ab initio* lattice thermal conductivity of MgO from a complete solution of the linearized Boltzmann transport equation**

Haruhiko Dekura (出倉春彦)¹ and Taku Tsuchiya (土屋卓久)^{1,2}

¹*Geodynamics Research Center, Ehime University, 2-5 Bunkyo-cho, Matsuyama, Ehime 790-8577, Japan*

²*Earth-Life Science Institute, Tokyo Institute of Technology, Tokyo 152-8550, Japan*

(Received 17 January 2017; revised manuscript received 21 April 2017; published 16 May 2017)

Lattice thermal conductivity κ_{lat} of MgO at high pressures P and temperatures T up to 150 GPa and 4000 K are determined using lattice dynamics calculations and the linearized phonon Boltzmann transport equation (BTE) beyond the relaxation time approximation (RTA) from first principles. It is found that the complete solution of the linearized BTE substantially corrects values of κ_{lat} calculated with the RTA by $\sim 30\%$, from ~ 42 to $\sim 54 \text{ W m}^{-1} \text{ K}^{-1}$ under ambient conditions. The calculated values of κ_{lat} are in good agreement with those from the existing experiments. At conditions representative of the Earth's core-mantle boundary ($P = 136 \text{ GPa}$ and $T = 3800 \text{ K}$), κ_{lat} is predicted to be ~ 32 and $\sim 40 \text{ W m}^{-1} \text{ K}^{-1}$ by RTA and the full solution of BTE, respectively. We report a detailed comparison of our study with earlier theoretical studies.

DOI: [10.1103/PhysRevB.95.184303](https://doi.org/10.1103/PhysRevB.95.184303)

I. INTRODUCTION

Lattice thermal conductivity κ_{lat} is one of the fundamental physical parameters in controlling the activity of heat transfer in a solid, and it attracts researchers from wide-ranging fields such as materials science, engineering, and Earth and planetary science [1–4]. The determination of κ_{lat} of Earth's constituent materials is key to understanding the dynamics and thermal evolution of the Earth's interior [5–7]. Despite their importance, studies on the measurement of κ_{lat} of the Earth's lower mantle minerals at high pressure (P) and temperature (T) have, so far, been limited, most likely due to technical difficulties in carrying out these experiments [8–11]. Therefore, extrapolation of κ_{lat} measured at much lower P and/or T than at the Earth's deep mantle and core conditions are often made to discuss physical properties at the Earth's deep interior [8,9,12–17].

In recent years, computational studies based on density functional theory (DFT) [18,19] have proved to be applicable in determining κ_{lat} under ambient conditions for many materials [20–25]. The techniques have also been applied to κ_{lat} of lower mantle minerals such as MgO (periclase) [26–29] and MgSiO₃ (bridgmanite) [30–32]. However, the earlier studies for MgO employed different techniques: de Koker applied equilibrium molecular dynamics (MD) simulations to extract phonon lifetimes by calculating the phonon spectral density [26,27], and Stackhouse *et al.* applied a nonequilibrium MD simulation technique, which directly determines heat flux \mathbf{Q} in a temperature gradient ∇T where κ_{lat} was estimated using Fourier's law $\mathbf{Q} = -\kappa_{\text{lat}} \nabla T$ [29]. Unlike these two MD-based methods, Tang *et al.* applied anharmonic lattice dynamics (ALD) to extract harmonic and anharmonic force constants (AFCs) [28]. Although these three approaches have determined values of κ_{lat} of MgO that are in good agreement with the available experimental data at low P , a quantitative mismatch in κ_{lat} among these studies exists at a high P (100 GPa) and T (2000 K) that is representative of deep lower mantle (e.g., $\sim 40 \text{ W m}^{-1} \text{ K}^{-1}$ [27], $\sim 30 \text{ W m}^{-1} \text{ K}^{-1}$ [29], and $\sim 60 \text{ W m}^{-1} \text{ K}^{-1}$ [28]). Consequently, this variation in the calculation of κ_{lat} along a

single geotherm renders κ_{lat} of MgO under the Earth's lower mantle conditions a current topic of debate.

The thermal transport properties of minerals in the Earth's interior are not clearly understood due to the limited number of studies available. For a better understanding of the physical behavior of κ_{lat} of minerals in the Earth's lower mantle, further theoretical and experimental investigations are required. Upon reviewing the *ab initio* computational methods applied to MgO [26–29], the method of Tang *et al.* has room for improvement from our point of view. They applied the relaxation time approximation (RTA) [1,33] to the linearized Boltzmann transport equation (BTE) for the variation in the phonon nonequilibrium distribution function, which drastically simplifies the original BTE. The RTA appears to substantially underestimate κ_{lat} (e.g., by $\sim 39\%$ in AlSb [23] and by $\sim 50\%$ in diamond [20] at room T and P). If κ_{lat} in MgO is also substantially underestimated, the correction by fully solving the BTE should be taken into account to better describe κ_{lat} of the Earth's lower mantle. In this paper, we calculated κ_{lat} of MgO by employing an iterative approach to fully solve the linearized BTE [34,35]. In this approach, the change in the phonon distribution functions due to the phonon-phonon scattering was taken into account. This method was found to work very well and provide a more rigorous description of anharmonic phonons and therefore of κ_{lat} [23,35]. We calculated P and T dependences of anharmonic phonon lifetimes and determined κ_{lat} of MgO for T and P up to 150 GPa and 4000 K, covering the entire lower mantle conditions based on *ab initio* ALD. We find that the correction to the RTA values of κ_{lat} is considerable, and thus, the full solution of BTE is a necessary requirement for determining thermal properties at Earth's deep mantle conditions.

II. PHONON TRANSPORT PROPERTIES

Heat conduction in MgO is predominantly due to phonons, and not electrons, because MgO is a pure insulator. ∇T induces heat flux $\mathbf{Q} = \sum_{\lambda} \hbar \omega_{\lambda} \mathbf{v}_{\lambda} n_{\lambda}$ through a sample [1]. The summation is over all phonon modes $\lambda = \{s, \mathbf{q}\}$, where \mathbf{q} is the phonon wave vector and s is the labeling index of the phonon

branch, ω_λ and $\mathbf{v}_\lambda = \nabla_{\mathbf{q}}\omega_\lambda$ are the phonon frequency and phonon group velocity, respectively, in mode λ . The phonon distribution function n_λ in the steady state obeys the BTE [33]

$$-\mathbf{v}_\lambda \cdot \nabla T \left(\frac{\partial n_\lambda}{\partial T} \right) + \left(\frac{\partial n_\lambda}{\partial t} \right)_{\text{scatt}} = 0. \quad (1)$$

The first term on the left-hand side represents the diffusion of n_λ due to the temperature gradient, and the second term is determined by the various scattering events, such as phonon-phonon scattering and phonon-defect scattering. The BTE normally leads to complicated simultaneous non-linear differential and integral equations, which makes the task of solving the BTE formidable. However, for a small ∇T , the BTE can be linearized in ∇T , and hence, the equation becomes easier to solve. For a small ∇T , n_λ is perturbed from its equilibrium state: $n_\lambda = n_\lambda^{(0)} + n_\lambda^{(1)}$, where $n_\lambda^{(0)} = 1/\{\exp(\hbar\omega_\lambda) - 1\}$ is the Bose-Einstein function. The fluctuation of the distribution function is linear in ∇T , $n_\lambda^{(1)} = -(\partial n_\lambda^{(0)}/\partial T)\mathbf{F}_\lambda \cdot \nabla T$. When only phonon-phonon scattering disturbs the distribution function, the resulting solution to the linearized BTE can be expressed as [34]

$$\mathbf{F}_\lambda = \tau_\lambda^{\text{RTA}}(\mathbf{v}_\lambda + \mathbf{\Delta}_\lambda), \quad (2)$$

where $\tau_\lambda^{\text{RTA}}$ is the phonon lifetime in phonon mode λ , which is commonly obtained using the RTA and regarded as the zeroth-order solution to the linearized BTE. The term $\mathbf{\Delta}_\lambda$, with dimensions of velocity, is an indicator of how well the full solution corrects the RTA prediction. In the framework of iterative method for solving the BTE, $\mathbf{\Delta}_\lambda$ is iteratively determined by the following set of coupled equations [34,35]:

$$\begin{aligned} \mathbf{\Delta}_\lambda \equiv & \frac{1}{N} \sum_{\lambda', \lambda''}^+ \Gamma_{\lambda\lambda'\lambda''}^+ (\xi_{\lambda\lambda'} \mathbf{F}_{\lambda''} - \xi_{\lambda\lambda''} \mathbf{F}_{\lambda'}) \\ & + \frac{1}{2N} \sum_{\lambda', \lambda''}^- \Gamma_{\lambda\lambda'\lambda''}^- (\xi_{\lambda\lambda'} \mathbf{F}_{\lambda''} + \xi_{\lambda\lambda''} \mathbf{F}_{\lambda'}), \end{aligned} \quad (3)$$

where N is the number of unit cells, which is equivalent to that of \mathbf{q} points sampled in the first Brillouin zone, and $\xi_{\lambda\lambda'} \equiv \omega_{\lambda'}/\omega_\lambda$. $\Gamma_{\lambda\lambda'\lambda''}$ represents the phonon scattering rate due to the phonon-phonon interaction, which is calculated based on second-order perturbation theory for the three-phonon process [33]. In Eq. (3), the sums are over the phase space of λ' and λ'' that satisfy the phonon energy and momentum conservation condition for the difference (-) or summation (+) process in the three-phonon scattering [21,36]: $\hbar\omega_\lambda \pm \hbar\omega_{\lambda'} = \hbar\omega_{\lambda''}$ and $\hbar\mathbf{q} \pm \hbar\mathbf{q}' - \hbar\mathbf{q}'' = \mathbf{G}$, where \mathbf{G} is the reciprocal vector, which is a zero vector for Normal (N) process or nonzero vector for resistive umklapp (U) processes [1]. Here, $\tau_\lambda^{\text{RTA}}$ is given by

$$(\tau_\lambda^{\text{RTA}})^{-1} = \frac{1}{N} \left(\sum_{\lambda', \lambda''}^+ \Gamma_{\lambda\lambda'\lambda''}^+ + \frac{1}{2} \sum_{\lambda', \lambda''}^- \Gamma_{\lambda\lambda'\lambda''}^- \right), \quad (4)$$

where the mathematical form of $\Gamma_{\lambda\lambda'\lambda''}^\pm$ is [33]

$$\begin{aligned} \Gamma_{\lambda\lambda'\lambda''}^\pm &= \frac{\hbar\pi}{4\omega_\lambda\omega_{\lambda'}\omega_{\lambda''}} \left(n_{\lambda'}^{(0)} - n_{\lambda''}^{(0)} \right) \\ &\quad \times | \psi_{\lambda\lambda'\lambda''}^\pm |^2 \delta(\omega_\lambda \pm \omega_{\lambda'} - \omega_{\lambda''}). \end{aligned} \quad (5)$$

In Eq. (5), the three-phonon matrix element $\psi_{\lambda\lambda'\lambda''}$, is expressed as

$$\begin{aligned} \psi_{\lambda\lambda'\lambda''} &= \sum_{kk'k''} \sum_{\alpha\beta\gamma} \sum_{\ell'\ell''} \Phi_{ijk}^{\alpha\beta\gamma}(0k, \ell'k', \ell''k'') \\ &\quad \times \frac{e_{\alpha k}^\lambda e_{\beta k'}^{\lambda'} e_{\gamma k''}^{\lambda''}}{\sqrt{M_k M_{k'} M_{k''}}} e^{i(\mathbf{q}' \cdot \mathbf{R}_{\ell'} + \mathbf{q}'' \cdot \mathbf{R}_{\ell''})}, \end{aligned} \quad (6)$$

where $\Phi_{ijk}^{\alpha\beta\gamma} = (\frac{\partial^3 E}{\partial r_i^\alpha \partial r_j^\beta \partial r_k^\gamma})_0$ is the third-order internal AFC. Here, E is the adiabatic potential of the system calculated using DFT. The atomic indices are i, j , and k , and the Cartesian components are α, β , and γ . r_i^α is the α th component of the equilibrium position of the i th ion. Also, $e_{\alpha k}^\lambda$ represents the α th component of the phonon eigenvector of the k th atom in the unit cell with an ionic mass M_k in λ . At the initial conditions, the second term on the right-hand side of Eq. (2) was set to zero. The n th iterative solution $\mathbf{\Delta}_\lambda^{(n)}$ was calculated iteratively using Eq. (3) from the set of the $(n-1)$ th solution of $\{\mathbf{F}_\lambda^{(n-1)}, \Gamma_{\lambda\lambda'\lambda''}^\pm\}$. The sequence was considered to converge when $|\Delta_{\lambda\alpha}^{(n)}/\Delta_{\lambda\alpha}^{(n-1)}| \approx 1$ was achieved. Then \mathbf{F}_λ and n_λ were completely determined for all λ . The lattice thermal conductivity tensor $\kappa_{\alpha\beta}$ is defined as a response of the heat current along α , Q_α , to the first-order temperature gradient along β [33], i.e., $Q_\alpha = -\sum_\beta \kappa_{\alpha\beta}(\partial T/\partial x_\beta)$, where $\kappa_{\alpha\beta}$ is defined as

$$\kappa_{\alpha\beta} = \frac{1}{k_B T^2 \Omega N} \sum_\lambda n_\lambda^{(0)} (n_\lambda^{(0)} + 1) (\hbar\omega_\lambda)^2 v_{\lambda\alpha} F_{\lambda\beta}, \quad (7)$$

where Ω is the crystal volume of the unit cell. The cubic symmetry ensures that $\kappa_{\alpha\beta}$ is of the diagonal form [37]: $\kappa_{\alpha\beta} = \bar{\kappa} \delta_{\alpha\beta}$, where $\bar{\kappa} \equiv (\kappa_{xx} + \kappa_{yy} + \kappa_{zz})/3$ is the scalar quantity of $\kappa_{\alpha\beta}$ averaged over the crystallographic axes. Therefore, in this paper, we denote $\bar{\kappa}$ as κ_{lat} . We have used the ShengBTE package [38] in solving the BTE using the iterative scheme [34].

In this paper, we carried out *ab initio* electronic and lattice dynamics simulations for NaCl-type MgO. The adiabatic potential (total energy) and thermal equation of states (EoS) were calculated based on the DFT and density functional perturbation theory (DFPT) [39] using the Quantum ESPRESSO package [40]. We applied the local density approximation [41] for both the DFT and DFPT calculations using norm-conserving-type, and ultrasoft-type pseudopotentials for Mg and O, respectively. These potentials have been well tested in our previous research [42–44]. The Kohn-Sham eigenfunctions were expanded with a 50 Ry of kinetic cutoff energy on a $6 \times 6 \times 6$ Monkhorst-Pack \mathbf{k} -point mesh [45]. A $6 \times 6 \times 6$ uniform mesh was used to sample \mathbf{q} points for which the phonon calculations were performed using DFPT. Here, $\Phi_{ijk}^{\alpha\beta\gamma}$ were calculated using a finite difference method [46] in real space following approaches of Refs. [25,47]:

$$\begin{aligned} \Phi_{ijk}^{\alpha\beta\gamma} &= \left(\frac{\partial^3 E}{\partial r_i^\alpha \partial r_j^\beta \partial r_k^\gamma} \right)_0 \\ &\approx \frac{1}{2\delta u} \left[\left(\frac{\partial^2 E}{\partial r_j^\beta \partial r_k^\gamma} \right)_{r_i^\alpha = \delta u} - \left(\frac{\partial^2 E}{\partial r_j^\beta \partial r_k^\gamma} \right)_{r_i^\alpha = -\delta u} \right] \\ &\approx \frac{1}{4\delta u^2} \left[-f_k^\gamma \{r_i^\alpha = \delta u, r_j^\beta = \delta u\} + f_k^\gamma \{r_i^\alpha = \delta u, r_j^\beta = -\delta u\} \right. \\ &\quad \left. + f_k^\gamma \{r_i^\alpha = -\delta u, r_j^\beta = \delta u\} - f_k^\gamma \{r_i^\alpha = -\delta u, r_j^\beta = -\delta u\} \right], \end{aligned} \quad (8)$$

where δu is a small displacement from the equilibrium position, and f_k^γ is the γ component of the force acting on the k th ion. A number of self-consistent field calculations to determine the AFCs got drastically reduced due to the space group symmetry and permutation symmetry in $\Phi_{ijk}^{\alpha\beta\gamma}$. In the calculation, we have used $\delta u = 0.01 \text{ \AA}$ in a $3 \times 3 \times 3$ rhombohedral supercell (54 atoms). The phase space of three-phonon scattering rates $\Gamma_{\lambda\lambda'\lambda''}^\pm$ [see Eq. (5)] were computed on a $16 \times 16 \times 16$ uniform \mathbf{q} -point mesh, both for the N and U processes. For the energy conservation described as the delta function in Eq. (5), we used an adaptive broadening scheme [48].

The convergence of $\Gamma_{\lambda\lambda'\lambda''}$ [Eq. (5)] with respect to a cutoff distance (R_c) for the AFCs in real space must be carefully examined because insufficiently small R_c leads to underestimation of $\Gamma_{\lambda\lambda'\lambda''}$, which in turn leads to overestimation of κ_{lat} . Here, κ_{lat} with respect to R_c were checked from nearest-neighbor (NN) to seventh NN at 300 K at the static zero-pressure density of 3.62 g cm^{-3} . The calculated κ_{lat} was found to vary greatly from $274 \text{ W m}^{-1} \text{ K}^{-1}$ (first NN), $92 \text{ W m}^{-1} \text{ K}^{-1}$ (third NN), $67 \text{ W m}^{-1} \text{ K}^{-1}$ (fifth NN), and $64 \text{ W m}^{-1} \text{ K}^{-1}$ (seventh NN) $\text{W m}^{-1} \text{ K}^{-1}$. This clearly indicates that at least the fifth NN AFCs have to be considered in order to obtain good convergence. All the AFCs up to the seventh NN were therefore included in all the calculations of κ_{lat} of MgO in this paper.

At an even more stringent condition with a $4 \times 4 \times 4$ supercell (128 atoms) with AFCs up to eighth NN shells and a $24 \times 24 \times 24$ \mathbf{q} -point mesh, we observed that κ_{lat} differs by only 3%. In addition, we find that, for $\delta u = 0.012 \text{ \AA}$, κ_{lat} varies up to 10 and 3% for 0 and 100 GPa, respectively. These conditions ensure numerical accuracy in the computations performed in this paper.

III. RESULTS AND DISCUSSION

We calculated phonon lifetimes determined using the RTA ($\tau_\lambda^{\text{RTA}}$). Figure 1 shows $\tau_\lambda^{\text{RTA}}$ as a function of the phonon frequencies ω_λ , at 300 K at 0 and 100 GPa. We observed that $\tau_\lambda^{\text{RTA}}$ tends to diverge as ω_λ decreases to zero, which may be a typical phenomenon at relatively low T [22,25,49]. In the midrange frequencies, $\tau_\lambda^{\text{RTA}}$ has a small frequency dependence, while a substantial decrease in $\tau_\lambda^{\text{RTA}}$ is observed at higher frequencies corresponding to optical phonons. These behaviors may be understood in terms of variations of three-phonon anharmonic decay channels. To account for the decay channels, we calculated the two-phonon density of states (TDoS) defined for difference D^- and summation D^+ processes given by

$$D^\pm(\omega_\lambda) = \frac{1}{N} \sum_{\lambda', \lambda''} \delta(\omega_{\lambda'} \pm \omega_{\lambda''} - \omega_\lambda). \quad (9)$$

The difference process clearly dominates the three-phonon scattering at low frequencies, whereas the summation process becomes dominant at high frequencies. The TDoS is found to decrease as P increases, as shown in Fig. 1(b), indicating that phonon scattering decreases at high P . This is consistent with our observation that $\tau_\lambda^{\text{RTA}}$ of each mode increases with increasing P . The T dependence of $\tau_\lambda^{\text{RTA}}$ can be understood in terms of the Bose factor $n_\lambda^{(0)}$ in Eq. (5). At T much higher

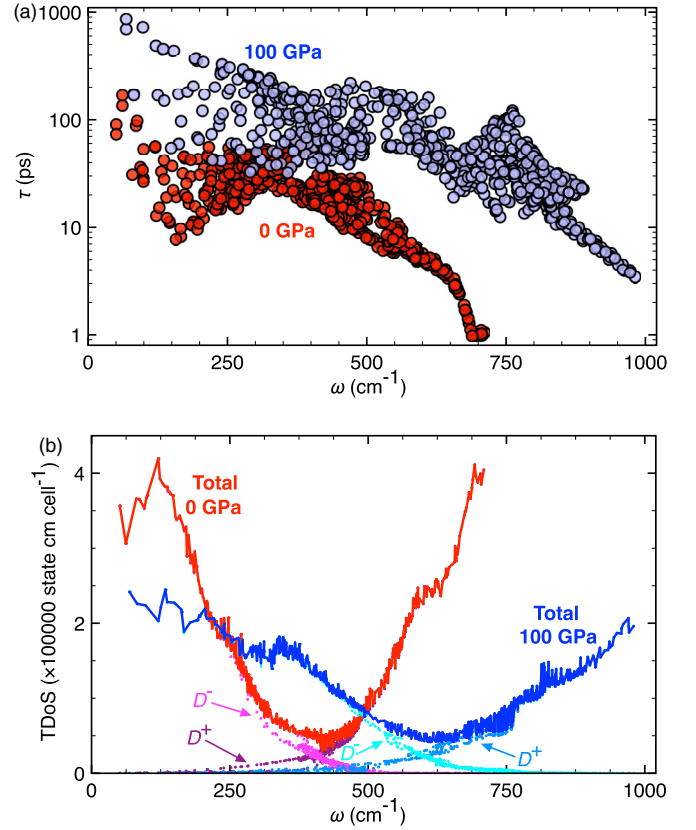


FIG. 1. (a) Anharmonic phonon lifetimes τ of MgO obtained using the RTA at 300 K. (b) Two-phonon densities of states (TDoSs) calculated for difference (D^-) and summation (D^+) processes at 0 and 100 GPa. The total TDoSs ($= D^- + D^+$) are also shown.

than the Debye temperature θ_D , the three-phonon scattering rate $\Gamma \propto \tau_{\text{RTA}}^{-1}$ is linear in T , resulting from the T dependence of the Bose factor, which results in a reciprocal T dependence in $\tau_{\text{RTA}} \propto \Gamma^{-1} \propto T^{-1}$.

Using the calculated $\tau_\lambda^{\text{RTA}}$ combined with a dataset of ω_λ and \mathbf{v}_λ , $\kappa_{\text{lat}}(\rho, T)$ was computed as a function of density ρ and T , as shown in Fig. 2. The full solution to the BTE is also shown in Fig. 2. The density range here corresponds to the static P from -10 to 150 GPa. Our results were found to fit the following analytical function well, as shown in Fig. 2:

$$\kappa_{\text{lat}}(\rho, T) = \kappa_0 x^q \left(\frac{1 - e^{-a_3 \frac{T_{\text{ref}}}{T}}}{1 - e^{-a_3}} \right), \quad (10)$$

where $x \equiv \rho/\rho_{\text{ref}}$ and $q \equiv a_0 + a_1 x + a_2 x^2$. Here, κ_0 and $a_0 - a_3$ are the fitting parameters and were determined to have the following values: $\kappa_0 = 53.7 \pm 4.3 \text{ W m}^{-1} \text{ K}^{-1}$, $a_0 = 5.76$, $a_1 = 5.18$, $a_2 = -3.22$, and $a_3 = -0.0938$ for the full solution and $\kappa_0 = 42.2 \pm 3.8 \text{ W m}^{-1} \text{ K}^{-1}$, $a_0 = 5.90$, $a_1 = 5.26$, $a_2 = -3.34$, and $a_3 = -0.0637$ for the RTA. Here, $\rho_{\text{ref}} = 3.56 \text{ g cm}^{-3}$ is the density at 0 GPa and 300 K, and $T_{\text{ref}} = 300 \text{ K}$ is the reference temperature. We found that this fitting produced a relative error of $\sim 8\%$. As discussed in the subsequent paragraph, the full solutions (solid lines in Fig. 2) substantially improve the RTAs (dashed lines in Fig. 2). The obtained analytical representation of $\kappa_{\text{lat}}(\rho, T)$ was then converted into a representation dependent on P and

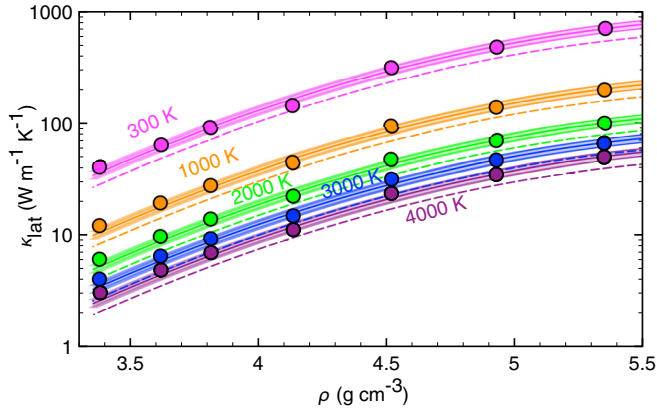


FIG. 2. Density ρ dependence of lattice thermal conductivity κ_{lat} calculated for temperatures between 300 and 4000 K. The full converged solution is plotted with regression curves calculated using Eq. (10) with a standard deviation of 8%, as indicated by the shaded bands. The calculation results obtained using the RTA are also provided (dashed lines).

T , $\kappa_{\text{lat}}(P, T)$, as depicted in Fig. 4, using the thermal EoS, $\rho(P, T)$, determined in the framework of DFPT combined with the quasiharmonic approximation (QHA) [42]. The behavior of $\kappa_{\text{lat}}(P, T)$ will be discussed in the following paragraphs.

We first compared our results with those of previous experimental and theoretical studies performed under ambient P , as shown in Fig. 3. The red solid line corresponds to the RTA results $\kappa_{\text{lat}}^{\text{RTA}}$, whereas the pink solid line represents the results obtained by fully solving the linearized BTE $\kappa_{\text{lat}}^{\text{full}}$. From Fig. 3, it is evident that the RTA solution substantially underestimates κ_{lat} for MgO. For example, at 300 K, $\kappa_{\text{lat}}^{\text{full}} \sim 53.7 \text{ W m}^{-1} \text{ K}^{-1}$ is approximately 30% higher than the RTA value $\kappa_{\text{lat}}^{\text{RTA}} \sim 42.2 \text{ W m}^{-1} \text{ K}^{-1}$. This modification is substantial compared with κ_{lat} of other materials, which show much smaller

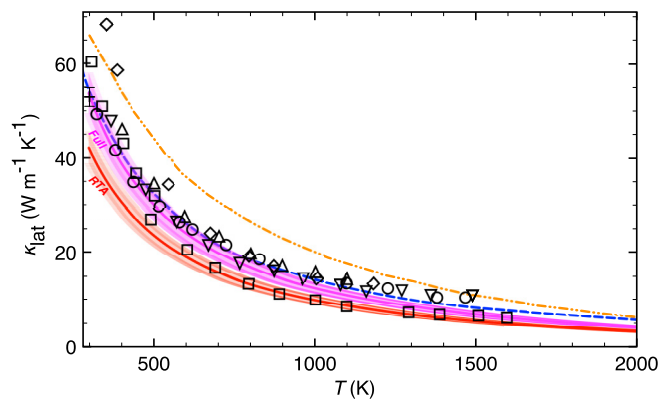


FIG. 3. Comparison of our calculated lattice thermal conductivity κ_{lat} of MgO with the results of existing experimental and theoretical studies under ambient pressure. The results of this paper (solid lines) with $1\sigma = 8\%$ confidence bands (shaded region) obtained using the RTA (red) and the full converged solution (pink) are compared with those of experiments (\square) [53], (\circ) [51], (Δ) [52], (\diamond) [50], (∇) [13], (+) [10], *ab initio* studies based on nonequilibrium MD simulations (dashed line) [29], and *ab initio* ALD simulations using the RTA without the isotopic correction (dashed double-dotted line) [28].

deviations; that is, they deviate by less than $\sim 10\%$ with respect to the RTA values, e.g., in intrinsic semiconductors (Si and Ge [21]) and compound semiconductors (AlP, GaN, GaP, GaAs, GaSb, InP, InAs, InSb, and AlN [23]), but comparable to diamond which has a $\sim 50\%$ deviation at room T [20]. This large correction to the RTA may come from weak U scattering. In the RTA, both the N and U processes are independent and enter in a purely resistive manner in the total three-phonon scattering rate, reflecting Matthiessen's rule [21] $1/\tau_{\lambda}^{\text{RTA}} = 1/\tau_{\lambda}^{(N)} + 1/\tau_{\lambda}^{(U)}$. Since the phonon heat transfer is principally carried out by phonons in the U scattering process [33], the full solution to the linearized BTE corrects this behavior. If the U process contribution is more considerable than the N process, the RTA approaches the full solution, so that the RTA well describes κ_{lat} [21]. On the other hand, if the U scattering is considerably weaker than the N scattering due to the smaller phase space for the three-phonon scattering rates in simple systems, such as that in the case of diamond [20], the contribution of the N scattering to the thermal resistivity using RTA is suitably wiped out through the iterative procedure in solving the linearized BTE. Then $\kappa_{\text{lat}}^{\text{RTA}}$ is largely corrected using the full solution. We assert that this is the case in our system, and consequently, our solution to the linearized BTE is important in accurately predicting κ_{lat} of MgO.

In Fig. 3, we found that our calculated values of κ_{lat} fall in the range of the scattering experimental data, between ~ 40 and $\sim 75 \text{ W m}^{-1} \text{ K}^{-1}$ [10,13,50–53]. A classical MD simulation has resulted, based on the Green-Kubo method [54], in a value of $\sim 110 \text{ W m}^{-1} \text{ K}^{-1}$, which is far from the experimental values. This disagreement may arise from two factors: (a) using empirical potentials, which may not easily describe the anharmonic interactions sensitive to the calculations of κ_{lat} , and (b) a fundamental limitation of the classical MD approach in describing ion dynamics at a temperature of 300 K, which is much lower than the θ_D of MgO ($\sim 1000 \text{ K}$ [55]), where quantum effects strongly control dynamical properties, including κ_{lat} . Compared with the *ab initio* MD simulations [27,29], our calculated $\kappa_{\text{lat}}^{\text{full}}$ is also in good agreement with previous studies within the numerical accuracy. On the other hand, an *ab initio* study based on the ALD using the RTA reported by Tang *et al.* [28] showed a $\kappa_{\text{lat}}^{\text{RTA}}$ value substantially larger than our values for $\kappa_{\text{lat}}^{\text{RTA}}$ and $\kappa_{\text{lat}}^{\text{full}}$. For example, at 300 K, they reported $\kappa_{\text{lat}}^{\text{RTA}}$ to be $\sim 100 \text{ W m}^{-1} \text{ K}^{-1}$, which is almost twice that of $\kappa_{\text{lat}}^{\text{full}}$ of $\sim 50 \text{ W m}^{-1} \text{ K}^{-1}$. They calculated the isotopic scattering based on the static perturbation theory [56,57] and included the effects to the total thermal resistivity using Matthiessen's rule, which takes into account mixing effects [33], and finally obtained a value of $\kappa_{\text{lat}}^{\text{RTA}} = 66 \text{ W m}^{-1} \text{ K}^{-1}$, which shifted the value much closer to the experimental values. Consequently, they argue that the disagreement in the phonon thermal conductivity with experiments resulted from lack of the isotopic scattering contribution. This seems, however, disputable from a computational point of view. Tang and Dong took into account only up to second NN AFCs to compute κ_{lat} [28,58]. As mentioned in Sec. II, this is, however, insufficient for the convergence and leads to a substantial overestimation in κ_{lat} . The considerable discrepancy between our κ_{lat} and Tang and Dong's with no isotopic correction should be attributed to the insufficient computational condition rather than to the lack of isotopic correction.

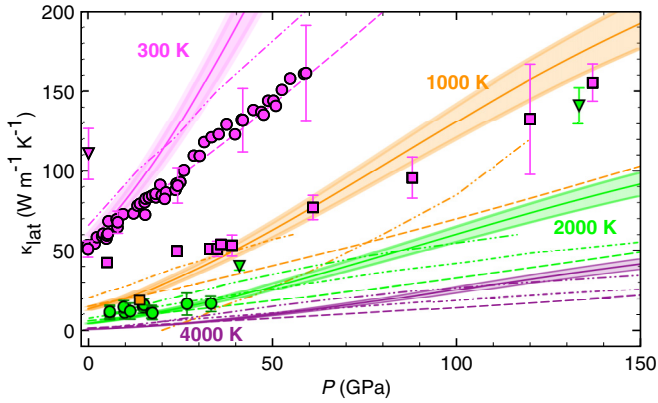


FIG. 4. Calculated κ_{lat} of MgO with the fully converged solutions to the linearized BTE (solid lines) as a function of pressure P at several T from 300 to 4000 K with $1\sigma = 8\%$ confidence bands (shaded regions). The results of previous studies based on *ab initio* ALD calculations with the isotopic correction (dashed double-dotted lines) [28], equilibrium (dash-dotted lines) [27] and nonequilibrium MD (dashed lines) [29], and experiments conducted using single-crystal samples (pink and green circles for 300 and 2000 K, respectively) [8,10] and polycrystalline samples (pink and orange squares for 300 and 1000 K, respectively) [9,17] are provided. The results of classical MD simulations (pink and green triangles for 300 and 2000 K, respectively) [54] are also depicted.

We now compare our results for κ_{lat} at high P and T with previous studies. Figure 4 shows our calculated $\kappa_{\text{lat}}^{\text{full}}$, alongside previous studies, as a function of P for several T from 300 to 4000 K. We note that large corrections to $\kappa_{\text{lat}}^{\text{RTA}}$ of $\sim 30\%$ from the full solution to the linearized BTE for MgO is geophysically important when discussing κ_{lat} using Earth’s lower mantle conditions to infer its thermal transport properties.

In comparing $\kappa_{\text{lat}}^{\text{full}}$ at 300 K and $P < 10$ GPa with the values reported previously, we found our results to agree well with those obtained in experiments using single crystals [10] and with *ab initio* calculations using nonequilibrium MD [29] and ALD with the isotopic correction [28]. In contrast, large discrepancies are evident between our predictions and the experimental values measured using a polycrystalline sample [17]. Imada *et al.* speculated that large discrepancies would result from the effects of phonon-grain boundary scattering on κ_{lat} [17]; however, they showed no direct evidence of these effects. Although quantitative evaluation is required, these effects may not have strong T dependence [49,53] and therefore may become negligible at high T . Phonon-phonon scattering is expected to dominate the thermal conduction in the Earth’s lower mantle temperature conditions ($T \gtrsim 1900$ K [59]). At higher P and 300 K, our calculated results deviate from those of the experiments using single crystals [10]. Although the cause of this deviation is unclear, it may be due to phonon scattering by crystal imperfections [33]. There could be a breakdown of samples to polycrystalline states or increase of dislocation density under the strong uniaxial stress [60] expected in room T diamond anvil cell experiments, which might result in thermal conductivity suppression at high P .

At $T = 2000$ K, the calculated $\kappa_{\text{lat}}^{\text{full}}$ values fall in the range of available experimental data at up to P of ~ 35 GPa [10], *ab initio* predictions determined using MD simulations [27,29], and ALD using the RTA [28]. However, as P increases, the difference in values between those in this paper and those of the previous studies [27,29] becomes very large, as shown in Fig. 4. For example, at 100 GPa and 2000 K, which is representative of Earth’s deep mantle conditions, our value is found to be $\sim 60 \pm 8$ $\text{W m}^{-1}\text{K}^{-1}$, whereas values of ~ 33 $\text{W m}^{-1}\text{K}^{-1}$ [29], ~ 40 $\text{W m}^{-1}\text{K}^{-1}$ [27], and ~ 54 $\text{W m}^{-1}\text{K}^{-1}$ [28] were reported previously. The classical MD simulation at 2000 K [54] yielded much higher conductivities, particularly at $P \sim 130$ GPa (Fig. 4), than this paper and previous *ab initio* MD studies [27,29]. Although the cause of these high conductivities is not clear, as mentioned in the previous paragraph, the use of empirical potentials may have affected the results. At Earth’s core-mantle boundary (CMB) conditions ($P = 136$ GPa and $T = 3800$ K [61]), $\kappa_{\text{lat}}^{\text{full}}$ is calculated to be 39.7 $\text{W m}^{-1}\text{K}^{-1}$, which corrects the RTA value predicted to be $\kappa_{\text{lat}}^{\text{RTA}} 31.6$ $\text{W m}^{-1}\text{K}^{-1}$. Our calculated $\kappa_{\text{lat}}^{\text{full}}$ is found to be larger than those obtained in previous *ab initio* MD simulations [27,29]; however, it is close to the value $\kappa_{\text{lat}}^{\text{RTA}} = 35$ $\text{W m}^{-1}\text{K}^{-1}$ with the isotopic correction reported by Tang *et al.* [28]. As the P dependence in κ_{lat} obtained at high P and T is completely different from that found in the data of Tang *et al.*, as demonstrated in Fig. 4, the agreement between the data of Tang *et al.* and our data is most likely coincidental. Differences in κ_{lat} at high P and T predicted by previous and present *ab initio* studies [27–29] may have resulted from errors in, for instance, numerical setup. Further studies, particularly experimental ones, are needed in order to assess reliability of the predicted results.

We will now discuss some potential limitations in our computations of κ_{lat} of MgO. Potential errors in κ_{lat} , particularly at high T , may be attributable to a breakdown of the QHA in describing the T dependence of ω_{λ} at high T . Previous *ab initio* studies on the thermodynamics of MgO (e.g., Ref. [62]), however, demonstrated that the QHA works well in determination of the thermal properties under Earth’s deep mantle conditions except at low P and high T . Also, the four-phonon (and higher-order) anharmonic scattering processes were ignored in the present calculations of the decay rate of n_{λ} . The reasonable agreements between the present calculations and previous experimental results imply that three-phonon scattering is dominant in MgO at lower mantle T . However, recent classical MD simulations yielded distinctive contributions of the four-phonon scattering by 15, 25, and 36% for diamond, Si, and Ge, respectively, which are typical highly conductive materials, even at 1000 K [63]. It might be worth extending our methods to higher-order anharmonic phonon scattering in the future.

IV. CONCLUSIONS

In conclusion, we calculated κ_{lat} for NaCl-type MgO at high P and T , up to 150 GPa and 4000 K, using *ab initio* ALD simulations. We solved the linearized BTE and corrected the values of κ_{lat} that were determined using the RTA. The full solution of the linearized BTE corrected the RTA values substantially, by about 30%, which indicates that

the anharmonic properties of MgO are governed by weak U phonon scattering, similar to the case of diamond. Therefore, a complete solution of the linearized BTE is essential to determine κ_{lat} of MgO. The κ_{lat} values obtained for MgO in this paper would help to model thermal transport properties of the Earth's deep interior.

ACKNOWLEDGMENTS

H.D. acknowledges Masahiro Osako, Tao Sun, and Masayuki Nishi for the valuable discussions. We appreciate

the anonymous reviewers for their helpful comments. The calculations were performed using resources of the High Performance Computing Infrastructure (HPCI) systems provided by Nagoya University (Project ID No. hp150047) and Tsukuba University (Project ID No. hp120155). This paper was supported by Ministry of Education, Culture, Sports, Science, and Technology MEXT KAKENHI Grant No. JP2628713 and JSPS KAKENHI (Grant No. 22224012) JSPS core to Core program on International Alliance for Material Science in Extreme States with High Power Laser and XFEL, and X-ray Free Electron Laser Priority Strategy Program (MEXT).

-
- [1] J. M. Ziman, *Electrons and Phonons* (Oxford University Press, London, 1960).
- [2] S. L. Shinde and J. S. Goela (eds.), *High Thermal Conductivity Materials* (Springer-Verlag, New York, 2006).
- [3] F. D. Stacey and P. M. Davis, *Physics of the Earth*, 4th ed. (Cambridge University Press, New York, 2008).
- [4] S. Lepri (ed.), *Thermal Transport in Low Dimensions from Statistical Physics to Nanoscale Heat Transfer* (Springer International Publishing, Basel, 2016).
- [5] T. Lay, J. Hernlund, and B. A. Buffett, *Nature Geosci.* **1**, 25 (2008).
- [6] D. L. Turcotte and G. Schubert, *Geodynamics*, 2nd ed. (Cambridge University Press, Cambridge, 1982).
- [7] D. Gubbins, A. P. Willis, and B. Sreenivasan, *Phys. Earth. Planet. Inter.* **162**, 256 (2007).
- [8] A. F. Goncharov, P. Beck, V. V. Struzhkin, B. D. Haugen, and S. D. Jacobsen, *Phys. Earth. Planet. Inter.* **174**, 24 (2009).
- [9] G. M. Manthilake, N. de Kocher, D. J. Frost, and C. A. Mammon, *Proc. Natl. Acad. Sci. USA* **108**, 17901 (2011).
- [10] D. A. Dalton, W. Hsieh, G. T. Bodensee, D. G. Cahill, and A. F. Gorchakov, *Sci. Rep.* **3**, 2400 (2013).
- [11] A. F. Gorchakov, S. S. Lebanon, X. Tan, G. T. Hohensee, D. G. Cahill, J. F. Lin, S. M. Thomas, T. Okuchi, and N. Tomioka, *Phys. Earth. Planet. Inter.* **247**, 11 (2015).
- [12] M. Osako and E. Ito, *Geophys. Res. Lett.* **18**, 239 (1991).
- [13] T. Katsura, *Phys. Earth. Planet. Inter.* **101**, 73 (1997).
- [14] M. Manga and R. Jeanloz, *J. Geophys. Res.* **102**, 2999 (1997).
- [15] A. M. Hofmeister, *Science* **283**, 1699 (1999).
- [16] K. Ohta, T. Yagi, N. Taketoshi, K. Hirose, T. Komabayashi, T. Baba, Y. Ohishi, and J. Hernlund, *Earth Planet. Sci. Lett.* **349–350**, 109 (2012).
- [17] S. Imada, K. Ohta, T. Yagi, K. Hirose, H. Yoshida, and H. Nagahara, *Geophys. Res. Lett.* **41**, 4542 (2014).
- [18] P. Hohenberg and W. Kohn, *Phys. Rev.* **136**, B864 (1964).
- [19] W. Kohn and L. J. Sham, *Phys. Rev.* **140**, A1133 (1965).
- [20] A. Ward, D. A. Broido, D. A. Stewart, and G. Deinzer, *Phys. Rev. B* **80**, 125203 (2009).
- [21] A. Ward and D. A. Broido, *Phys. Rev. B* **81**, 085205 (2010).
- [22] K. Esfarjani, G. Chen, and H. T. Stokes, *Phys. Rev. B* **84**, 085204 (2011).
- [23] L. Lindsay, D. A. Broido, and T. L. Reinecke, *Phys. Rev. B* **87**, 165201 (2013).
- [24] L. Paulatto, F. Mauri, and M. Lazzeri, *Phys. Rev. B* **87**, 214303 (2013).
- [25] A. Togo, L. Chaput, and I. Tanaka, *Phys. Rev. B* **91**, 094306 (2015).
- [26] N. de Koker, *Phys. Rev. Lett.* **103**, 125902 (2009).
- [27] N. de Koker, *Earth Planet. Sci. Lett.* **292**, 392 (2010).
- [28] X. Tang and J. Dong, *J. Proc. Natl. Acad. Sci. USA* **107**, 4539 (2010).
- [29] S. Stackhouse, L. Stixrude, and B. B. Karki, *Phys. Rev. Lett.* **104**, 208501 (2010).
- [30] H. Dekura, T. Tsuchiya, and J. Tsuchiya, *Phys. Rev. Lett.* **110**, 025904 (2013).
- [31] X. Tang, M. C. Ntam, J. Dong, E. S. G. Rainey, and A. Kavner, *Geophys. Res. Lett.* **41**, 2746 (2014).
- [32] S. Stackhouse, L. Stixrude, and B. B. Karki, *Earth Planet. Sci. Lett.* **427**, 11 (2015).
- [33] G. P. Srivastava, *The Physics of Phonons* (Adam Hilger, Philadelphia and New York, 1990).
- [34] M. Omini and A. Sparavigna, *Phys. Rev. B* **53**, 9064 (1996).
- [35] D. A. Broido, A. Ward, and N. Mingo, *Phys. Rev. B* **72**, 014308 (2005).
- [36] G. Deinzer, G. Birner, and D. Strauch, *Phys. Rev. B* **67**, 144304 (2003).
- [37] J. F. Nye, *Physical Properties of Crystals: Their Representation by Tensors and Matrices* (Oxford University Press, London, 1985).
- [38] <http://www.shengbte.org/>
- [39] S. Baroni, S. de Gironcoli, A. D. Corso, and P. Giannozzi, *Rev. Mod. Phys.* **73**, 515 (2001).
- [40] P. Giannozzi, S. Baroni, N. Bonini, M. Calandra, R. Car, C. Cavazzoni, D. Ceresoli, G. L. Chiarotti, M. Cococcioni, I. Dabo, A. Dal Corso, S. de Gironcoli, S. Fabris, G. Fratesi, R. Gebauer, U. Gerstmann, C. Gougoussis, A. Kokalj, M. Lazzeri, L. Martin-Samos *et al.*, *J. Phys. Condens. Matter.* **21**, 395502 (2009).
- [41] J. P. Perdew and A. Zunger, *Phys. Rev. B* **23**, 5048 (1981).
- [42] T. Tsuchiya and J. Tsuchiya, *Proc. Natl. Acad. Sci. USA* **108**, 1252 (2011).
- [43] X. Wang, T. Tsuchiya, and A. Hase, *Nature Geosci.* **8**, 556 (2015).
- [44] T. Sakai, H. Dekura, and N. Hirao, *Sci. Rep.* **6**, 22652 (2016).
- [45] H. J. Monkhorst and J. D. Pack, *Phys. Rev. B* **13**, 5188 (1976).
- [46] J. Stoer and R. Bulirsch, *Introduction to Numerical Analysis* (Springer-Verlag, New York, 1980).
- [47] L. Chaput, A. Togo, I. Tanaka, and G. Hug, *Phys. Rev. B* **84**, 094302 (2011).

- [48] J. R. Yates, X. Wang, D. Vanderbilt, and I. Souza, *Phys. Rev. B* **75**, 195121 (2007).
- [49] P. G. Klemens, *Proc. Phys. Soc. A* **68**, 1113 (1955).
- [50] F. R. Charvat and W. D. Kingery, *J. Am. Ceram. Soc.* **40**, 306 (1957).
- [51] G. A. Slack, *Phys. Rev.* **126**, 427 (1962).
- [52] H. Kanamori, N. Fujii, and H. Mizutani, *J. Geophys. Res.* **73**, 595 (1968).
- [53] Y. S. Touloukian, R. W. Powell, C. Y. Ho, and P. G. Klemens, *Thermophysical Properties of Matter - The TPRC Data Series. Volume 1. Thermal Conductivity - Metallic Elements and Alloys*, (IFI/Plenum, New York, 1970).
- [54] V. Haigis, M. Salanne, and S. Jahn, *Earth Planet. Sci. Lett.* **355-356**, 102 (2012).
- [55] D. G. Isaak, R. E. Cohen, and M. J. Mehl, *J. Geophys. Res.* **95**, 7055 (1990).
- [56] S. I. Tamura, *Phys. Rev. B* **27**, 858 (1983).
- [57] A. Kundu, N. Mingo, D. A. Broido, and D. A. Stewart, *Phys. Rev. B* **84**, 125426 (2011).
- [58] X. Tang and J. Dong, *Phys. Earth. Planet. Inter.* **174**, 33 (2009).
- [59] J. M. Brown and T. J. Shankland, *Geophys. J. R. Astron. Soc.* **66**, 579 (1981).
- [60] S. Karato and H. Jung, *Philos. Mag. A* **83**, 401 (2003).
- [61] K. Kawai and T. Tsuchiya, *Proc. Natl. Acad. Sci. USA* **106**, 22119 (2009).
- [62] B. B. Karki, R. M. Wentzcovitch, S. de Gironcoli, and S. Baroni, *Phys. Rev. B* **61**, 8793 (2000).
- [63] T. Feng and X. Ruan, *Phys. Rev. B* **93**, 045202 (2016).